Biogeosciences Discuss., 11, 16953–16992, 2014
www.biogeosciences-discuss.net/11/16953/2014/
doi:10.5194/bgd-11-16953-2014

Biogeosciences Discussions
Open Access

Modeling the impact of riverine DON removal by marine bacterioplankton on primary production in the Arctic Ocean

V. Le Fouest[1], M. Manizza[2], B. Tremblay[3], and M. Babin[4]

[1]Littoral Environnement et Sociétés, UMR 7266, Université de La Rochelle, La Rochelle, France
[2]Geosciences Research Division, Scripps Institution of Oceanography, University of California San Diego, La Jolla, CA, USA
[3]Department of Atmospheric and Oceanic Sciences, McGill University, Montreal, QC, Canada
[4]Takuvik Joint International Laboratory, Université Laval (Canada) & Centre National de la Recherche Scientifique (France), Département de Biologie, Québec, QC, Canada

Received: 30 October 2014 – Accepted: 14 November 2014 – Published: 9 December 2014

Correspondence to: V. Le Fouest (vincent.le_fouest@univ-lr.fr)

Published by Copernicus Publications on behalf of the European Geosciences Union.

Abstract

The planktonic and biogeochemical dynamics of the Arctic shelves exhibit a strong variability in response to Arctic warming. In this study, in order to elucidate on the processes regulating the production of phytoplankton (PP) and bacterioplankton (BP) and their interactions, we employ a biogeochemical model coupled to a pan-Arctic ocean-sea ice model (MITgcm) to explicitly simulate and quantify the contribution of usable dissolved organic nitrogen (DON) drained by the major circum-Arctic rivers on PP and BP in a scenario of melting sea ice (1998–2011). Model simulations suggest that on average between 1998 and 2011, the removal of usable RDON by bacterioplankton is responsible of a ∼ 26 % increase of the annual BP for the whole Arctic Ocean. With respect to total PP, the model simulates an increase of ∼ 8 % on an annual basis and of ∼ 18 % in summer. Recycled ammonium is responsible for the PP increase. The recycling of RDON by bacterioplankton promotes higher BP and PP but there is no significant temporal trend in the BP : PP ratio within the ice-free shelves over the 1998–2011 period. This suggests no significant evolution in the balance between autotrophy and heterotrophy in the last decade with a constant annual flux of RDON into the coastal ocean although changes in RDON supply and further reduction in sea ice cover could potentially alter this delicate balance.

1 Introduction

In response to the polar amplification of the global climate change, the rate of increase of air temperature in the lower atmosphere is twice as fast in the Arctic as in temperate regions. By the end of the century, model projections suggest an average increase of the surface air temperature of 3.7 °C relative to 1981–2000 (ACIA report, 2005). In response to Arctic warming, the plankton production and biogeochemistry in the Arctic Ocean (AO) evolves rapidly. Changes in phytoplankton communities (Li et al., 2009) and phenology in spring (Kahru et al., 2011) and fall (Ardyna et al., 2014) are observed.

BGD
11, 16953–16992, 2014

The AO tends to be overall more productive (Bélanger et al., 2013) and takes up more atmospheric carbon dioxide (1996–2007; Manizza et al., 2013). In the long term, model projections suggest an increase of spatially integrated primary production (PP) by the end of the 21st century (Vancoppenolle et al., 2013).

The AO is the basin the most influenced by continental freshwater. It receives 10 % of the freshwater that fluxes into the global ocean although representing only 1 % of the global ocean volume (Opshal et al., 1999). Circum-Arctic rivers are potentially a significant source of inorganic nutrients and organic matter for shelf seas (Le Fouest et al., 2013; Tank et al., 2012). 10 % of the global riverine inputs of organic carbon are conveyed into the AO (Rachold et al., 2004). This fraction is projected to increase in the near future due to the accelerated permafrost thawing (Frey et al., 2007). This pool of organic matter enters the carbon cycle but little is known about its fate and pathways within the plankton ecosystem in arctic waters prior to be exported into the Atlantic Ocean.

Bacterioplankton is a major biological component involved in the degradation and mineralization of dissolved organic matter in arctic waters (Retuerta-Ortega et al., 2012). It can significantly affect its fate and distribution within the entire water column (Bendsten et al., 2002) but also the microbial food web activity through the assimilation of remineralized nitrogen. However, the contribution of arctic bacterioplankton to plankton production in the context of Arctic warming remains an unknown. Despite the AO basin acts now as a sink of atmospheric carbon dioxide (1996–2007; Manizza et al., 2013), the balance between autotrophy and heterotrophy might change in the future based on the observed enhanced stratification of the water column (Li et al., 2009), the increase of sea temperature (Timmermans et al., 2014; Steele et al., 2008), acting as a key driver of arctic bacterioplankton metabolism (Piontek et al., 2014; Bendsten et al., 2002), and changes in the riverine inputs of nutrients driven by the increase of freshwater discharge (Shiklomanov and Lammers, 2011). In near-shore waters of the AO, riverine inputs already sustain part of the bacterial activity (e.g. Vallières et al., 2008).

BGD
11, 16953–16992, 2014

Using a relatively simple biogeochemical modeling approach, Tank et al. (2012) shed light on the potential impact of riverine nutrients inputs on the PP of the AO. In the present study, we propose to build from the static view provided by the work of Tank et al. (2012) by explicitly modeling the effect of the interactions between riverine dissolved organic nitrogen (RDON) and bacterioplankton on the PP in the AO. The objective is to use a pan-Arctic ocean-sea ice coupled model to quantify the contribution of usable RDON processed by marine bacterioplankton on its production and on the production of phytoplankton in a scenario of melting sea ice over the period 1998–2011.

2 Material and methods

2.1 The physical model

We used the MIT General Circulation model (MITgcm) (Marshall et al., 1997) coupled with a sea-ice model. The model is configured on a "cubed-sphere" grid encompassing the Arctic domain with open boundaries at $\approx 55^{\circ}$ N in the Atlantic and Pacific sectors. Prescribed boundary conditions for potential temperature, salinity, flow, and sea-surface elevation are provided from previous integrations of a global configuration of the same model (Menemenlis et al., 2005). The grid has a variable horizontal resolution with an average mesh of ~ 18 km. The mesh resolves major Arctic straits, including many of the channels of the Canadian Archipelago. The sea-ice and fluid dynamical equations are solved on the same horizontal mesh. The vertical grid is height based, varying from 10 m thick near the surface to ~ 450 m at a depth of ~ 6 km in 50 levels. Bathymetry is derived from the U.S. National Geophysical Data Center (NGDC) two-minute global relief data set (ETOPO2), which uses the International Bathymetric Chart of the Arctic Ocean (IBCAO) product for Arctic bathymetry (Jakobsson et al., 2008). The ETOPO2 data is smoothed to the model horizontal mesh and mapped to the ocean vertical levels using a "lopped cell" strategy (Adcroft et al., 1997), which permits accurate representation of the ocean bottom boundary.

BGD
11, 16953–16992, 2014

The ocean model's hydrography is initialized with observations taken from the Polar Science Center Hydrographic Climatology (PHC) 3.0 database (Steele et al., 2001). Initial sea-ice distributions are taken from the pan-Arctic Ice–Ocean Modeling and Assimilation System data sets (Zhang and Rothrock, 2003). Atmospheric forcings (10 m surface winds, 2 m air temperature and humidity, and downward long and short-wave radiation) are taken from the six hourly data sets of the Japanese 25 year ReAnalysis (JRA-25) (Onogi et al., 2007). Monthly mean estuarine fluxes of freshwater are based on the Arctic Runoff database (Lammers et al., 2001; Shiklomanov et al., 2000). The sea-ice component of the coupled model follows the viscous-plastic rheology formulation of Hibler (1979) with momentum equations solved implicitly on a C-grid (Arakawa and Lamb, 1977) using a procedure based on Zhang and Hibler (1997). Fluxes of momentum into ice due to the overlying atmospheric winds and momentum fluxes between sea-ice and the ocean are calculated by solving for the momentum balance at each surface grid column (Hibler and Bryan, 1987). This model configuration was previously used to study the Arctic freshwater budget (Condron et al., 2009). Modeling studies of Condron et al. (2009) compared to observations by Serreze et al. (2006) concluded that this model configuration is able to realistically represent the freshwater budget of the AO, including import and export of freshwater from the Bering and Fram straits and from the Canadian Archipelago.

2.2 The riverine DON (RDON) discharge

In this study, in order to realistically represent in our biogeochemical model the RDON flux in the AO we follow the approach adopted by Manizza et al. (2009) based on seasonally-explicit regression relationships. These relationships use co-variations between water yield and dissolved organic carbon (DOC) concentrations in circum-Arctic rivers to define RDOC monthly-averaged fluxes for 10 regions around the pan-Arctic domain. These regions are the Barents Sea, Kara Sea, Laptev Sea, East Siberian Sea, Chukchi Sea, Bering Strait, Beaufort Sea, Canadian Archipelago, Hudson Bay, and Hudson Strait using published watershed areas and seasonal water runoff (Lammers

BGD
11, 16953–16992, 2014

et al., 2001). The approach use empirical relationships quantifying the co-variation between discharge and riverine DOC (RDOC) to scale the Lammers et al. (2001) discharge estimates into estimates of RDOC export. Estimates of RDOC export for December–March, April–July, and August–November were divided into monthly bins according to measured distributions of RDOC export for those months in Arctic rivers. For each season, [RDOC]-discharge relationships were developed with North American and Eurasian rivers considered separately. Data from the Yukon, Mackenzie, and Kuparuk rivers were used to define a runoff-[RDOC] relationship for drainage areas in North America, and data from the Ob', Yenisey, and Lena rivers were used to define a runoff-[RDOC] relationship for drainage areas in Eurasia. RDOC for the Yenisey, Ob', Lena, and Mackenzie were collected as part of the Pan-Arctic River Transport of Nutrients, Organic Matter, and Suspended Sediments (PARTNERS) project (McClelland et al., 2008). RDOC concentrations for the Kuparuk River were collected as part of the NSF Study of the Northern Alaska Coastal System (SNACS, http://www.arcus.org/arcss/snacs/products). In all cases, discharge data were acquired from ArcticRIMS (http://rims.unh.edu/). Recent sampling efforts on these rivers have provided exceptional seasonal coverage (McClelland et al., 2008) and the total annual discharge of RDOC in the model is 37.7 $TgC\,yr^{-1}$, which is consistent with the estimate of Raymond et al. (2007). To initialize the model, we use the three-dimension RDOC field obtained from the 3 decade integration of the model by Manizza et al. (2009). After that time, RDOC distributions are relatively steady, because the flushing time for tracers through the surface waters of the basin is on the order of a decade. RDOC was converted into nitrogen currency (RDON) using a molar C : N ratio of 40 : 1 (Tank et al., 2012.; Köhler et al., 2003). We assume that 15 % of the RDON entering the model at river grid cells is usable by bacterioplankton (e.g. Wickland et al., 2012).

2.3 The biogeochemical model

We couple to the MITgcm physical model a biogeochemical model that explicitly represents the plankton ecosystem dynamics. The biogeochemical model is improved from

BGD
11, 16953–16992, 2014

previous applications in sub-Arctic (Le Fouest et al., 2005, 2006) and Arctic waters (Le Fouest et al., 2011, 2013b). In the model nitrogen is the currency and it includes 10 compartments (i.e., nine in the pelagic domain + RDON that couples the marine and terrestrial cycling of nitrogen) chosen according to the ecosystem structure observed in the AO. Phytoplankton is size-fractionated into large (> 5 µm) and small (< 5 µm) phytoplankton (LP and SP, respectively). The two zooplankton compartments represent large (LZ, mainly copepods) and small (SZ, protozooplankton) organisms. Dissolved inorganic nutrients are nitrate (NO_3) and ammonium (NH_4). Detrital (i.e. produced by the biogeochemical model components) particulate and dissolved organic nitrogen (dPON and dDON, respectively) close the nitrogen cycle. Bacterioplankton (BACT) are explicitly represented following the model of Fasham et al. (1990). They grow on NH_4, dDON and on the usable fraction of RDON (see Appendix for details). LP and SP growth depends on light, NO_3 and NH_4 availability according to the Liebig's law of minimum. LZ graze on LP and SZ, whereas SZ graze on SP and BACT. Fecal pellets and LP basal mortality fuel the dPON pool. The dDON pool is made of unassimilated nitrogen resulting from SZ grazing, SP, SZ and BACT basal mortality and dPON fragmentation. BACT release, LZ excretion and unassimilated nitrogen resulting from SZ grazing are the sources of NH_4 in the model. NH_4 is converted into NO_3 through the nitrification process. For phytoplankton, nitrogen is converted into carbon using the Redfield carbon to nitrogen (C : N) molar ratio (106 : 16; Redfield et al., 1963) and into Chl using variable C : Chl mass ratios computed according to a modified version of the phytoplankton photoacclimation model of Cloern et al. (1995). The plankton biogeochemical model (Fig. 1) is fully detailed in the Appendix. Differential equations are given in Table 1, whereas biological parameters are given in Table 2.

Nitrate data used for the model initialization are from the World Ocean Atlas 2005 (National Oceanographic Data Centre, 2006). LP and SP are assigned a constant field over the model grid (0.2 and 0.002 mmol N m^{-3} in the top eighth layers and below, respectively) (e.g. Sherr et al., 2003; Ducklow, 1999; Taniguchi, 1999). Same conditions are imposed for BACT (e.g. Sherr et al., 2003; Ducklow, 1999). LZ and SZ are assigned

BGD
11, 16953–16992, 2014

a constant field over the model grid (0.1 and 0.001 mmol N m^{-3} in the top eighth layers and below, respectively) (e.g. Sherr et al., 2003; Taniguchi, 1999). Same conditions are imposed a priori for dPON. A value of 1 mmol N m^{-3} of NH_4 (e.g. Kristiansen et al., 1994) and dDON (e.g. Charria et al., 2008) is imposed at each grid cell. Boundary conditions at the North Atlantic and North Pacific sectors are data from the World Ocean Atlas 2005 (NODC, 2006) for NO_3, and null for the remaining 9 biogeochemical tracers. Apart from RDON, there are no riverine inputs for the remaining 9 biogeochemical tracers.

2.4 Coupled model integrations

The model is spun up by repeating twice the decade January 1980–December 1989. It is thereafter initialized with the physical and biogeochemical fields obtained from 31 December 1989 to run the 1990–2011 time period. Two simulations are then carried out: without usable RDON removal by bacterioplankton (our control run, hereafter CTRL run) and with usable RDON removal by bacterioplankton (hereafter RIV run). The difference between the two simulations provides information on the potential impact of the interactions between bacterioplankton and usable RDON on bacterioplankton production (BP), nutrients regeneration, and ultimately primary production (PP) in the Arctic basin.

3 Results

3.1 Primary production

Shelf seas influenced the least by riverine inputs of RDON show comparable simulated annual rates of total PP in the CTRL and RIV runs (Fig. 2). In the Barents Sea, simulated PP averaged over 1998–2011 reaches up to ~ 80 g C m^{-2} yr^{-1} in line with previous remote sensing estimates (up to 70–80 g C m^{-2} yr^{-1} in average over 1998–

BGD
11, 16953–16992, 2014

2010; Bélanger et al., 2013). In the central Chukchi Sea, simulated PP lies between 50–80 g C m^{-2} yr^{-1} in agreement with the observed range (15–80 g C m^{-2} yr^{-1} in average over 1998–2007; in Bélanger et al., 2013).

The largest differences in total PP between the two runs are found in the river-influenced Eurasian seas (East-Siberian Sea, Laptev Sea, and Kara Sea) (Fig. 2). In the CTRL run, maximum simulated PP rates reach ~ 30 g C m^{-2} yr^{-1}, which is more than 3-fold lower than satellite-derived and in-situ estimates that can exceed 100 g C m^{-2} yr^{-1} (Bélanger et al., 2013; Codispoti et al., 2013; Sakshaug, 2004). In contrast, PP rates simulated in RIV run (80–90 g C m^{-2} yr^{-1}) show a better agreement with observations.

The increase of the 1998–2011 averaged annual PP in RIV run relative to CTRL run is due to the increase of NH_4-supported PP (Fig. 3d–f). In contrast, new PP remains overall unaffected by the bacterial use of RDON (Fig. 3a–c). In the Kara Sea, Laptev Sea, East-Siberian Sea, and Beaufort Sea, simulated new PP is mostly < 20 g C m^{-2} yr^{-1}, in agreement with previously estimated rates (< 17 g C m^{-2} yr^{-1}; Sakshaug, 2004). New PP rates simulated by the model in the more productive areas are also in line with Sakshaug's estimated rates. In the Chukchi Sea, new PP lies generally in the 10–30 g C m^{-2} yr^{-1} range and reaches > 100 g C m^{-2} yr^{-1} at the sea opening (5–160 g C m^{-2} yr^{-1}; Sakshaug, 2004). Simulated new PP is up to ~ 70 g C m^{-2} yr^{-1} in the Barents Sea close to the value given by Sakshaug (up to 100 g C m^{-2} yr^{-1}; 2004). In the Greenland Sea and Labrador Sea, the simulated new PP rates are ~ 50 and ~ 30 g C m^{-2} yr^{-1}, respectively (40–45 g C m^{-2} yr^{-1}; Sakshaug, 2004).

Direct estimates of NH_4-supported PP based on measurements are rare in Arctic coastal waters. Nevertheless, they can be crudely derived by subtracting new PP from total PP estimated by Sakshaug (2004). In the Eurasian and North American shelves, NH_4-supported PP in CTRL run is overall < 10 g C m^{-2} yr^{-1} (Fig. 3d). This is low relative to the rates derived from Sakshaug's data, which would range between ~ 25 and ~ 40 g C m^{-2} yr^{-1}. By contrast, in RIV run, rates simulated in offshore shelf waters are

BGD
11, 16953–16992, 2014

$\sim$ 10–30 g C m^{-2} yr^{-1} but, closer to the coast, reach locally 40–50 g C m^{-2} yr^{-1} (Laptev Sea) and 70–80 g C m^{-2} yr^{-1} (Kara Sea) (Fig. 3e).

Averaged over 1998–2011, the total PP simulated by the model and integrated over the whole AO is 662 $\pm$ 91 TgC yr^{-1} in CTRL run and 717 $\pm$ 95 TgC yr^{-1} in RIV run. These values are within the range of previously reported rates based on remote sensing or in-situ data (385–1008 TgC yr^{-1}, Bélanger et al., 2013; Codispoti et al., 2013; Hill et al., 2013; Arrigo and van Dijken, 2011). Between the two model runs, the annual total PP increased by $\sim$ 8 % in average over 1998–2011. In September–October, when the simulated sea ice concentration reaches its seasonal minimum, the total PP increase is more than twice ($\sim$ 18 %, in average).

3.2 Bacterioplankton activity

The PP increase it tightly linked to a higher bacterioplankton activity that promotes RDON recycling into nutrients usable by both phytoplankton and bacterioplankton. The bacterioplankton biomass (BB), integrated between the sea surface and 50 m and averaged over April to June (spring) and July to September (summer), is shown in Fig. 4. As for PP, the Barents and Chukchi seas show comparable levels of BB in CTRL run and RIVR run. In the Chukchi Sea, the BB simulated in spring ($<$ 100–250 mgC m^{-2}; Fig. 4a and b) overlaps with the measured range (222–358 mgC m^{-2}; Kirchman et al., 2009). It is similar in summer, when simulated ($\sim$ 100 to $>$ 800 mgC m^{-2}; Fig. 4d and e) and measured BB levels (250–507 mgC m^{-2}; Kirchman et al., 2009; Steward et al., 1996) are higher than in spring. In the Barents Sea, the simulated BB increases from $<$ 100 mgC m^{-2} in spring to $<$ 250 mgC m^{-2} in summer to fall within the measured range (from $\sim$ 80 mgC m^{-2} in spring to $\sim$ 400 mgC m^{-2} in summer, in average; Sturluson et al., 2008). In the highly river-influenced shelf seas, the two runs show notable differences in their simulated BB (Fig. 4c and f). In the central part of the Kara Sea influenced by the Ob' and Yenisey River plumes, BB measured in late summer along a south–north transect from the Yama Peninsula to the Novaya Zemlya island is reported to range be-

BGD
11, 16953–16992, 2014

tween ~ 0.1 and 7 mgC m^{-3} (Sazhin et al., 2010). For the same time period and along a comparable transect, simulated values of BB are < 2 mgC m^{-2} in CTRL run. However, in RIV run, BB increases up to ~ 6–7 mgC m^{-3} to match the values measured in Sazhin et al. (2010).

The depth-integrated (0–50 m) bacterioplankton production (BP) simulated in both CTRL and RIV runs in summer in the Chukchi Sea (< 280 mgC m^{-2} d^{-1}) is consistent with measurements reported in this season (5–301 mgC m^{-2} d^{-1}; Kirchman et al., 2009; Rich et al., 1997; Steward et al., 1996). In the Beaufort Sea area influenced by the Mackenzie River plume, the simulated BP is lower than ~ 6 mgC m^{-2} d^{-1} in CTRL run, which is much below measurements made within the area (25–68 mgC m^{-2} d^{-1}; Ortega-Retuerta et al., 2012; Vallières et al., 2008). By contrast, in RIV run, simulated BP (< 30 mgC m^{-2} d^{-1}) gets closer to the lower range of observations. Similarly, BP simulated in CTRL run in the Kara Sea (< 30 mgC m^{-2} d^{-1}) does not exceed the first mid-range of measurements given by Meon and Amon (12–79 mgC m^{-2} d^{-1}; 2004). In RIV run, the simulated BP (~ 4–90 mgC m^{-2} d^{-1}) overlaps the measured range (12–79 mgC m^{-2} d^{-1}; Meon and Amon, 2004) to reach locally up to 120 mgC m^{-2} d^{-1}. This result is consistent with enrichment experiments conducted with surface oceanic water sampled in the Beaufort Sea that showed a 43 % increase of BP when Mackenzie River water was added in samples (see Ortega-Retuerta et al., 2012).

Averaged over 1998–2011, the total BP simulated by the model and integrated over the whole AO is, in average, 26 % higher in RIV run (68 ± 9 TgC yr^{-1}) than in CTRL run (54 ± 8 TgC yr^{-1}). Bacterioplankton recycle RDON into nutrients that can be used back by both phytoplankton and bacterioplankton hence promoting their growth. In addition, bacterioplankton and small phytoplankton are grazed by microzooplankton that, in turn, are grazed by mesozooplankton. More organic matter is channeled towards the upper trophic levels, a flow that also contributes to fuel the dDON and NH_4 pools through recycling. By enabling the removal of RDON by bacterioplankton in the biogeochemical model, the biomass of microzooplankton and mesozooplankton, averaged over 1998–2011, increased by ~ 16.1 and 43.6 %, respectively.

BGD
11, 16953–16992, 2014

3.3 The bacterioplankton production vs. primary production ratio (BP : PP)

The BP : PP ratio is computed over the AO shelf, delimited here by the 200 m isobaths, for ice-free waters (i.e. with less than 30 % of ice cover). In average for the 1998–2011 period, the simulated BP : PP ratio is 0.19 ± 0.02 in CTRL run and 0.21 ± 0.01 in RIV run. These values lie within the range observed in open (0.02; Kirchman et al., 2009) and coastal waters (0.37–0.43; Ortega-Retuerta et al., 2012; Garneau et al., 2008). When looking at the temporal evolution of BP : PP in RIV run (Fig. 5), the model simulates a significant increase of PP ($r = 0.57$, $p < 0.05$) and BP ($r = 0.63$, $p < 0.05$) between 1998 and 2011, with a production maximum simulated in 2007, the year showing the higher sea ice minimum. However, there is no evidence of a significant temporal trend of BP : PP ($r = -0.09$, $p > 0.05$) over 1998–2011. This result suggests that, with a constant annual flux of RDON into the coastal AO, the significant increase in simulated BP in the model is not high enough to promote a higher contribution of heterotrophy with respect to autotrophy within the upper water column.

4 Discussion

The coupled model suggests that NH_4 produced from the remineralization of RDON by the microbial food web contributes by ∼ 8 % to the annual pan-Arctic PP over 1998–2011. This is about twice the value given in the study of Tank et al. (2012) that, in addition to RDON, accounted for the contribution of riverine inorganic nutrients as well as of the photochemical transformation of RDON into NH_4. In our coupled model, the uptake of RDON by marine bacterioplankton and its subsequent recycling into reduced nitrogen is the sink term that shapes, with ocean transport, the spatial and temporal distribution of RDON. The photoammonification process is not parameterized but, if so, it would fuel the stock of NH_4 available for phytoplankton and bacterioplankton use, particularly in summer (e.g. Le Fouest et al., 2013; Xie et al., 2013). The RDON contri-

BGD
11, 16953–16992, 2014

bution to plankton production simulated by the coupled model can thus be considered as a minimum estimate.

From the total input of RDON, only a fraction is directly usable by the plankton (e.g. Wickland et al., 2012). This fraction that enters the coupled model by the 10 river source points is set to 15 % of the total RDON input according to the study of Wickland et al. (2012), which suggests that about 15 % of the total RDON pool can be degraded within less than one month. This value was chosen based on annual averages calculated from measurements or from model outputs for the Mackenzie River, Yukon River, Kolyma River, Lena River, Yenisey River, and Ob' River (e.g. Wickland et al., 2012). Note, however, that the average values given in Wickland et al. (2012) vary among seasons and rivers. They are the lowest in the Lena River (8 %) and the highest in the Ob' River (19 %). Maximum values as high as 24 % of usable RDON are reported for the Ob' River. Sensitivity analyses with different parameterizations of the usable RDON fraction set amongst river and seasons would hence be informative on the amplitude of the response of PP and BP to spatial and temporal variations of the RDON inputs. Nevertheless, the use a constant fraction provides a first order estimation of the RDON contribution to BP and PP that is consistent with the average state of knowledge on the RDON inputs.

In the biogeochemical model, the usable RDON, dDON, and NH_4 produced by the plankton components are taken up by bacterioplankton to build up biomass. In order to synthetize cell proteins, bacterioplankton require at least carbon and nitrogen. As a nitrogen-based model, carbon is obtained from usable RDON (RDOC converted into nitrogen currency) and dDON while nitrogen is provided by NH_4 recycled within the microbial food web. The growth function of bacterioplankton is formulated using the Fasham et al. (1990) model, which assumes that in a balanced growth situation the ratio of NH_4 uptake to DON uptake is constant to ensure that bacterioplankton biomass of the required C : N ratio is produced from DON with a given C : N ratio. In the model equations, the uptake rate of both DON and NH_4 decreases if there is not enough NH_4 available (refer to Eqs. 19–20 and Eq. 22 in the Appendix) hence translat-

BGD
11, 16953–16992, 2014

ing both nitrogen and energy limitation. In Arctic waters, the inhibition of DOC uptake by bacterioplankton under inorganic nitrogen limitation has been shown by Thingstad et al. (2008). However, as DON is used as a proxy of DOC, it assumes a constant C : N ratio of the substrate. As a consequence, any explicit stoichiometric treatment of the bacterioplankton metabolism is precluded in the model as well as any stoichiometric coupling between DOC and inorganic nutrients (e.g. Thingstad et al., 2008). Making the C : N ratio of the substrates of terrigeneous and/or marine origin vary in a realistic way in biogeochemical models would hence farther be required. However, the parameterization of variable C : N ratio is not trivial as it requires large in-situ datasets (see Letscher et al., 2014) and, in Arctic river-influenced shelf seas, a good knowledge on the characteristics of the terrigenous dissolved organic matter flowing into the coastal ocean (e.g. Mann et al., 2012). In the meantime, the coupled model that is used in the present study offers an interesting alternative to more complex (in terms of number of biological equations and parameters) models of bacterioplankton growth applied to shelf waters (e.g. Auger et al., 2011; Anderson and Williams, 1998).

In the biogeochemical model, bacterioplankton compete with phytoplankton for the NH_4 remineralized from the usable RDON and dDON pools. This competition for nutrient resource acts as a bottom-up control of the simulated phytoplankton and bacterioplankton production and, finally, of the BP : PP ratio. By contrasts with bacterioplankton, phytoplankton uptake of inorganic nutrients is also limited by light. In the model, the diffuse attenuation of the incident light caused by the pool of coloured dissolved organic matter ($0.05\,m^{-1}$) is set as constant in the model. It results that light attenuation in the water column is same in river plumes as in open and clearer waters. However, river plumes transfer to the coastal marine environment large amounts of optically-active coloured dissolved organic matter of terrigenous origin that strongly attenuate the incident light propagation with depth. As the model does not take into account for the stronger light attenuation in river plumes, it may cause an overestimation of the simulated phytoplankton growth on NH_4 recycled from RDON by bacterioplankton and an underestimation of BP in rive plumes. As a consequence, the spatial and temporal evo-

BGD
11, 16953–16992, 2014

lution of the simulated BP : PP ratio can be impacted on shelves. In addition, the ability of Arctic phytoplankton to assimilate low molecular weight DON compounds (50 % of total nitrogen assimilated annually; see Simpson et al., 2013) is likely to play also an important role in the phytoplankton-bacterioplankton competition on shelves. A more accurate representation of the simulated underwater light field and nutrients uptake in river plumes in the coupled model will certainly improve its ability to simulate the competition for nutrients between phytoplankton and bacterioplankton, and hence to predict the temporal evolution of the BP : PP ratio within Arctic waters.

5 Conclusions

A pan-Arctic physical-biogeochemical model was used to quantify the contribution of usable dissolved organic nitrogen drained by the major pan-Arctic rivers on marine bacterioplankton and phytoplankton production in a scenario of melting sea ice (1998–2011). When accounting for the removal of RDON by bacterioplankton in the coupled model, the ability to predict PP and BP in river-influenced shelves is improved. The key points of the study are:

1. In average between 1998 and 2011, the removal of usable RDON by bacterioplankton is responsible of an increase by ∼ 26 % of the annual BP, and of an increase by ∼ 8 % of the total annual PP.

2. Recycled ammonium is responsible for the total PP increase; total summertime PP is increased by ∼ 18 %, in average, over 1998–2011.

3. The processing of usable RDON by bacterioplankton promotes a higher annual BP and PP but there is no significant temporal trend in the BP : PP ratio over 1998–2011 on the ice-free shelves; this suggests no significant evolution in the balance between autotrophy and heterotrophy in the last decade with a constant annual flux of RDON into the coastal ocean.

BGD
11, 16953–16992, 2014

The effect of the predicted warming on the Arctic watersheds is linked to a potential regional increase of the RDON inputs into the AO shelf by 32–53 % by the end of the century (Frey et al., 2007). Combined with the accelerated sea ice decline (Comiso et al., 2008) and the increase of seawater temperature on Arctic shelves (Timmermans et al., 2014), this new biogeochemical and physical setting might exacerbate the competing effect for resources between autotrophs and heterotrophs as sea ice recedes in summer. As a consequence, the metabolic state of the AO shelves could be altered. Nevertheless, to obtain robust predictions of the response of the microbial food web functioning and mass fluxes, coupled models would require improvements in the parameterized land-ocean fluxes in terms of spatial and temporal variability of the freshwater discharge and nutrients fluxes. In their study combining in-situ datasets and modeling, Holmes et al. (2011) show that annual fluxes of RDOC in the Lena River estimated between 1999 and 2008 can vary by about a 2-fold factor. Such variations point out the significance of considering the short-term and inter-annual variability of the continental fluxes into the coastal ocean to draw temporal trends in plankton production and investigate potential changes in trends related to the Arctic warming. Finally, model predictions of future trajectories of PP (e.g. Vancoppenolle et al., 2013) would probably gain in considering riverine nutrients fluxes as an important driver of PP on Arctic shelves for the next decades.

Appendix A:

The set of differential equations that include the mechanistic formulations cited below is given in Table 1. The biological parameters related to the mathematical equations are detailed in Table 2.

BGD
11, 16953–16992, 2014

A1 Phytoplankton

The growth rate ($\mu^{LP,SP}$, d^{-1}) of large and small phytoplankton (LP and SP, respectively) depends on both light and nitrogen availability. It is computed according to the Liebig's Law of the minimum between the nutrient-based and light-based growth rates ($\mu_N^{LP,SP}$ and $\mu_{light}^{LP,SP}$, respectively):

$$\mu^{LP,SP} = \left(\mu_N^{LP,SP}, \mu_{light}^{LP,SP}\right) \tag{A1}$$

The nutrient-based growth rate is computed as follows:

$$\mu_N^{LP,SP} = \mu_{max}^{LP,SP} \lim_N^{LP,SP} \tag{A2}$$

where $\mu_{max}^{LP,SP}$ is the maximum growth rate and $\lim_N^{LP,SP}$ the total nutrient limitation term (dimensionless) computed according to the substitutable model of O'Neill et al. (1989):

$$\lim_N^{LP,SP} = \frac{NO_3 K_{NH_4}^{LP,SP} + NH_4 K_{NO_3}^{LP,SP}}{NO_3 K_{NH_4}^{LP,SP} + NH_4 K_{NO_3}^{LP,SP} + K_{NH_4}^{LP,SP} K_{NO_3}^{LP,SP}} \tag{A3}$$

$$\lim_{NO_3}^{LP,SP} = \frac{NO_3 K_{NH_4}^{LP,SP}}{NO_3 K_{NH_4}^{LP,SP} + NH_4 K_{NO_3}^{LP,SP}} \tag{A4}$$

$$\lim_{NH_4}^{LP,SP} = \frac{NH_4 K_{NO_3}^{LP,SP}}{NO_3 K_{NH_4}^{LP,SP} + NH_4 K_{NO_3}^{LP,SP}} \tag{A5}$$

where $\lim_{NO_3}^{LP,SP}$ and $\lim_{NH_4}^{LP,SP}$ are the nitrate (NO_3) and ammonium (NH_4) uptake fractions, respectively. $K_{NH_4}^{LP,SP}$ and $K_{NO_3}^{LP,SP}$ are the half-saturation for NH_4 and NO_3 uptake,

BGD
11, 16953–16992, 2014

respectively. NH_4 is set to be the preferred inorganic nitrogen source (Dorch, 1990) with a higher affinity for SP (Tremblay et al., 2000). This is expressed in the model by half-saturation constants for NH_4 uptake ($K_{NH_4}^{LP,SP}$) significantly lower than for NO_3 that, when used with the substitutable model, allow for an inhibitory effect of NH_4 on NO_3 uptake as often observed (Dorch, 1990). It implies that NO_3 uptake by diatoms and flagellates is inhibited by NH_4 at concentrations two-fold and ten-fold lower than NO_3 concentrations, respectively. The equation used to compute the light-based growth rate is:

$$\mu_{light}^{LP,SP} = \mu_{max}^{LP,SP} \lim_{light}^{LP,SP} \quad \text{(A6)}$$

where $\lim_{light}^{LP,SP}$ is the light limitation term (dimensionless) expressed as:

$$\lim_{light}^{LP,SP} = 1 - e^{-\frac{E_Z}{E_k^{LP,SP}}} \quad \text{(A7)}$$

where $E_k^{LP,SP}$ is the light saturation parameter (Ein $m^{-2} d^{-1}$) computed as follows:

$$E_k^{LP,SP} = \left(\frac{C}{Chl}\right)^{LP,SP} \frac{\mu_{max}^{LP,SP}}{\alpha_{LP,SP}} \quad \text{(A8)}$$

where C : Chl is the carbon to Chl ratio ($g\,g^{-1}$) and $\alpha_{LP,SP}$ is the initial slope ($mg\,C\,(mg\,Chl)^{-1}\,(Ein\,m^{-2}\,d^{-1})^{-1}$) of the photosynthesis-irradiance curve. Photoacclimation translates the adaptative response through varying C : Chl ratios in response to light and nutrient availability (e.g. Cloern et al., 1995; Geider et al., 1997; MacIntyre et al., 2002).

Varying C : Chl ratios are computed using a modified version of the empirical relationship of Cloern et al. (1995) successfully applied to Hudson Bay in the Arctic (Sibert

BGD
11, 16953–16992, 2014

et al., 2011). The ratios can vary up to 4- to 6-fold based on the general photoacclimation rule given by MacIntyre et al. (2002) and on Arctic nano- and picophytoplankton data (DuRand et al., 2002; Sherr et al., 2003) as follows:

$$\left(\frac{\text{Chl}}{\text{C}}\right)^{\text{LP}} = \left(\frac{\text{Chl}}{\text{C}}\right)^{\text{LP}}_{\text{max}} \left(1 + 4e^{-0.5\frac{E_z}{K_E^{\text{LP}}}} \lim_{\text{N}}^{\text{LP}}\right) \quad \text{(A9)}$$

$$\left(\frac{\text{Chl}}{\text{C}}\right)^{\text{SP}} = \left(\frac{\text{Chl}}{\text{C}}\right)^{\text{SP}}_{\text{max}} \left(1 + 5e^{-0.5\frac{E_z}{K_E^{\text{SP}}}} \lim_{\text{N}}^{\text{SP}}\right) \quad \text{(A10)}$$

where $K_E^{\text{LP,SP}}$ is the half-saturation parameter driving the curvature of the C : Chl vs. light relationship. E_z (Ein m^{-2} d^{-1}) is the downwelling PAR propagating according to the Beer–Lambert's law:

$$E_z = \text{PAR0} \int e^{-[(k_{\text{chl}} + k_w + k_{\text{nonchl}})z]} \text{d}z \quad \text{(A11)}$$

where the diffuse attenuation of PAR with depth (z) is due to the simulated Chl (kchl) (m^{-1}; Morel, 1988), water molecules (k_w) (0.04 m^{-1}; Morel, 1988) and non-chlorophyllous matter (k_{nonchl}). k_{nonchl} is set to 0.05 m^{-1}. kchl is calculated according to Morel et al. (1988) as follows:

$$\text{kchl} = 0.0518\text{Chl}^{-0.572}\text{Chl} \quad \text{(A12)}$$

with

$$\text{Chl} = 12\left(\frac{106}{16}\right)\left[\left(\frac{\text{Chl}}{\text{C}}\right)^{\text{LP}}\text{LP} + \left(\frac{\text{Chl}}{\text{C}}\right)^{\text{SP}}\text{SP}\right] \quad \text{(A13)}$$

Apart from grazing, phytoplankton loss terms include basal mortality and sinking for LP. LP sinking rates vary in the model from 0 to 2 m d^{-1} depending on nutrients availability (Bienfang et al., 1983):

$$\text{sed}_{\text{lp}} = \text{sed\_lp}\left(1 - \lim_{\text{N}}^{\text{LP}}\right) \quad \text{(A14)}$$

BGD
11, 16953–16992, 2014

A2 Zooplankton

Mathematical formulations and parameters related to large zooplankton (LZ) dynamics were chosen to reflect copepods as they dominate in abundance at the study station (Forest et al., 2012). Grazing (d^{-1}) is described by an Ivlev function:

$$G_{LZ} = G_{LZ}^{max}\left[\left(1 - e^{-\lambda(LP+SZ)}\right)\right] \quad \text{(A15)}$$

LZ grazes upon LP and protozooplankton (SZ) with a prey-specific grazing rate assumed to be proportional to the relative biomass of the prey (Campbell et al., 2009) defined for LP as follows:

$$pf_{LP} = \frac{LP}{LP + SZ} \quad \text{(A16)}$$

Losses in LZ biomass are due to NH_4 release, fecal pellets production (non-assimilated nitrogen ingested) and mortality. Mortality is assumed to be mainly due to predation (Eiane et al., 2002) and is described by a density-dependant quadratic function. The latter implicitly represents cannibalism as well as predation by appendicularians (Forest et al., 2012) and limits the occurrence of oscillations generated in such non-linear systems (Edwards and Bees, 2001). The constant of mortality is set to 0.2 $(\text{mmol N m}^{-3})^{-1}$ to simulate realistic mortality rates (e.g. Ohman et al., 2004).

SZ grazing upon SP and bacterioplankton (BACT) is formulated by a sigmoid "Holling-type-III" function:

$$G_{SZ} = G_{SZ}^{max}\frac{(SP + BACT)^2}{(SP + BACT)^2 + K_G^2} \quad \text{(A17)}$$

The function provides a threshold-like limit for low SP biomass that enhances the biological system stability (e.g. Steele and Henderson, 1992). In polar waters, there is evidence that protozooplankton exert a control on small phytoplankton biomass only

BGD
11, 16953–16992, 2014

beyond a threshold (Lancelot et al., 1997). As for LZ, SZ graze upon both SP and BACT with a prey-specific grazing rate (d^{-1}) assumed to be proportional to the relative biomass of the prey defined for SP as follows:

$$pf_{SP} = \frac{SP}{SP + BACT} \quad \text{(A18)}$$

According to the study of Riegman et al. (1993), we set the fraction of food ingested by SZ and being converted into biomass to 30 %. Lehrter et al. (1999) report that > 30 % of the total nitrogen release by SZ could be in the dissolved organic form. In the model, assuming that 40 % is released as labile DON (dDON), the remaining 60 % are lost as NH_4. Remaining SZ loss terms are grazing by LZ and mortality. Similarly to LZ, mortality is expressed by a density-dependent quadratic function to represent grazing amongst SZ.

A3 Bacterioplankton

Bacterioplankton is explicitly simulated following the model of Fasham et al. (1990). They use for growth NH_4, dDON and usable RDON. Usable RDON is considered as 15 % of total RDON (e.g. Wickland et al., 2012) and is converted into Nitrogen currency (RDON) using a C : N ratio of 40 (Tank et al., 2012; Köhler et al., 2003). DONl (i.e. the sum of dDON and usable RDON) is the preferred substrate for bacterial uptake (d^{-1}) (Kirchman et al., 1989) represented by a Michaelis–Menten model:

$$Ubact_{DONl} = Ubact_{max} BACT \left(\frac{DONl}{K^{BACT}_{DONl} + S + DONl} \right) Q_{10} \quad \text{(A19)}$$

where $Ubact_{max}$ is the maximum uptake rate, $K^{BACT}_{NH_4,DONl}$ ($mmol\,N\,m^{-3}$) is the half-saturation constant for uptake and S the total nitrogenous substrate ($mmol\,N\,m^{-3}$) defined as:

$$S = (NH_4, 0.6DONl) \quad \text{(A20)}$$

BGD
11, 16953–16992, 2014

According to Bendtsen et al. (2002) works in the Greenland Sea, a Q_{10} function was introduced using a Q_{10}-factor of 3 (Kirchman et al., 2005):

$$Q_{10} = 3^{\frac{T}{10}} \tag{A21}$$

where T is the simulated seawater temperature. A temperature normalized maximum growth rate of $1\,d^{-1}$ was used to simulate maximum growth rates in line with those measured in polar waters (e.g. Nedwell and Rutter, 1994). A growth efficiency of 20 % (Ortega-Retuerta et al., 2012; Meon and Amon, 2004) was imposed.

Similarly, the uptake of NH_4 is represented as follows:

$$\mathrm{Ubact}_{NH_4} = \mathrm{Ubact}_{max}\mathrm{BACT}\left(\frac{S}{K_{NH_4}^{BACT} + S + \mathrm{DONl}}\right)Q_{10} \tag{A22}$$

This formulation ensures that the uptake of NH_4 will be 0.6 times the uptake of DONl, as required by the balanced growth model (e.g. Fasham et al., 1990). Such a mechanistic behavior is consistent with the preferential uptake of DONl relative to NH_4 (Kirchman, 1990). Basal mortality is in the NH_4 form and represents 5 % of the biomass.

A4 Detritus

The pool of detrital particulate organic nitrogen (dPON) is fueled by LZ fecal pellets production and by LZ and LP mortality. The sedimentation loss term (d^{-1}) is expressed as a quadratic function allowing for increasing implicit aggregation of particles with increasing dPON concentrations:

$$\mathrm{sed}_{pon} = \mathrm{sed\_dponPON} \tag{A23}$$

where sed_dpon is the sedimentation constant ($m\,d^{-1}\,(mmol\,N\,m^{-3})^{-1}$). The second loss term is the dPON fragmentation into dDON (e.g. Grossart and Ploug, 2001).

The dDON pool results from dPON fragmentation, SP, SZ, and BACT basal mortality and SZ release. It is explicitly remineralized into NH_4 by bacterioplankton.

BGD
11, 16953–16992, 2014

A5 Nutrients

NH_4 resulting from the remineralization by BACT and from the LZ and SZ release fuels regenerated primary production and BACT production. In turn, NH_4 is undergoes nitrification (d^{-1}) into NO_3 as follows:

$$\text{nitrif} = \text{nitrif}_{\max}\left(\frac{NH_4}{NH_4 + K^N_{\text{nitrif}}}\right)\left(1 - \frac{E_z}{E_z + K^{\text{light}}_{\text{nitrif}}}\right) \quad \text{(A24)}$$

Where $\text{nitrif}_{\max}$ is the maximum nitrification rate and K^N_{nitrif} and $K^{\text{light}}_{\text{nitrif}}$ the half-saturation constants for NH_4 (mmol N m^{-3}) and light ($\text{Ein m}^{-2}\,\text{d}^{-1}$) use, respectively. The latter is defined as a fraction of surface PAR (E_0) as follows:

$$K^{\text{light}}_{\text{nitrif}} = 0.005E_0 \quad \text{(A25)}$$

Mean values taken from the literature (Guerrero and Jones, 1996; Olson, 1981a, b) are used to set parameters.

Acknowledgements. VLF also acknowledges support from the European Space Agency and the Centre national d'études spatiales (CNES) as part of the MALINA project, funded by the Institut national des sciences de l'univers – Centre national de la recherche scientifique (CYBER/LEFE and PICS programmes), the Agence nationale de la recherche and the CNES. MB is supported by the Canada Excellence Research Chair in "Remote sensing of Canada's new Arctic frontier". The authors wish to thank Oliver Jahn from MIT for having kindly provided MITgcm biogeochemical boundary data.

References

Arctic Climate Impact Assessment: Arctic Climate Impact Assessment, Cambridge Press Univ., New York, 1042 pp., 2005.

BGD
11, 16953–16992, 2014

Adcroft, A., Hill, C., and Marshall, J.: Representation of topography by shaved cells in a height coordinate ocean model, Mon. Weather Rev., 125, 2293–2315, 1997.
Anderson, T. R., and Williams, P. J. L.: Modelling the seasonal cycle of dissolved organic carbon at Station E1 in the English Channel, Estuar. Coast. Shelf S., 46, 93–109, 1998.
Arakawa, A. and Lamb, V.: Computational design of the basic dynamical processes of the UCLA general circulation model, Methods Comput. Phys., 17, 174–267, 1977.
Ardyna, M., Babin, M., Gosselin, M., Devred, E., Rainville, L., and Tremblay, J.-E.: Recent Arctic Ocean sea ice loss triggers novel fall phytoplankton blooms, Geophys. Res. Lett., 41, 6207–6212, doi:10.1002/2014GL061047, 2014.
Arrigo, K. R. and van Dijken, G. L.: Secular trends in Arctic Ocean net primary production, J. Geophys. Res., 116, C09011, doi:10.1029/2011JC007151, 2011.
Auger, P. A., Diaz, F., Ulses, C., Estournel, C., Neveux, J., Joux, F., Pujo-Pay, M., and Naudin, J. J.: Functioning of the planktonic ecosystem on the Gulf of Lions shelf (NW Mediterranean) during spring and its impact on the carbon deposition: a field data and 3-D modelling combined approach, Biogeosciences, 8, 3231–3261, doi:10.5194/bg-8-3231-2011, 2011.
Bélanger, S., Babin, M., and Tremblay, J.-É.: Increasing cloudiness in Arctic damps the increase in phytoplankton primary production due to sea ice receding, Biogeosciences, 10, 4087–4101, doi:10.5194/bg-10-4087-2013, 2013.
Bendsten, J., Lundsgaard, C., Middelboe, M., and Archer, D.: Influence of bacterial uptake on deep-ocean dissolved organic carbon, Global Biogeochem. Cy., 16, 1127, doi:10.1029/2002GB001947, 2002.
Bienfang, P., Szyper, J., and Laws, E.: Sinking rate and pigment responses to light limitation of a marine diatom: implications to dynamics of chlorophyll maximum layers, Oceanol. Acta, 6, 55–62, 1983.
Bendtsen, J., Lundsgaard, C., Middelboe, M., and Archer, D.: Influence of bacterial uptake on deep-ocean dissolved organic carbon, Global Biogeochem. Cy., 16, 1127, doi:10.1029/2002GB001947, 2002.
Campbell, R. G., Sherr, E. B., Ashjian, C. J., Plourde. S., Sherr, B. F., Hill, V., and Stockwell, D. A.: Mesozooplankton prey preference and grazing impact in the western Arctic Ocean, Deep-Sea Res. Pt. II, 56, 1274–1289, doi:10.1016/j.dsr2.2008.10.027, 2009.
Charria, G., Dadou, I., Llido, J., Drévillon, M., and Garçon, V.: Importance of dissolved organic nitrogen in the north Atlantic Ocean in sustaining primary production: a 3-D modelling approach, Biogeosciences, 5, 1437–1455, doi:10.5194/bg-5-1437-2008, 2008.

BGD
11, 16953–16992, 2014

Cloern, J. E., Grenz, C., and Videgar-Lucas, L.: An empirical model of the phytoplankton chlorophyll : carbon ratio – the conversion factor between productivity and growth rate, Limnol. Oceanogr., 40, 1313–1321, 1995.
Codispoti, L. A., Kelly, V., Thessen, A., Matrai, P., Hill, V., Steele, M., and Light, B.: Synthesis of primary production in the Arctic Ocean: III. Nitrate and phosphate based estimates of net community production, Prog. Oceanogr., 110, 126–150, doi:10.1016/j.pocean.2012.11.006, 2013.
Condron, A., Winsor, P., Hill, C. N., and Menemenlis, D.: Response of Arctic freshwater budget to extreme NAO forcing, J. Climate, 22, 2422–2437, 2009.
Comiso, J. C., Parkinson, C. L., Gersten, R., and Stock, L.: Accelerated decline in the Arctic sea ice cover, Geophys. Res. Lett., 35, L01703, doi:10.1029/2007GL031972, 2008.
Dorch, Q.: The interaction between ammonium and nitrate uptake in phytoplankton, Mar. Ecol.-Prog. Ser., 61, 183–201, 1990.
Ducklow, H. W.: The bacterial component of the oceanic euphotic zone, FEMS Microbiol. Ecol., 30, 1–10, 1999.
DuRand, M. D., Green, R. E., Sosik, H. M., and Olson, R. J.: Diel variations in Optical properties of Micromonas pusilla (Prasinophyceae), J. Phycol., 38, 1132–1142, 2002.
Edwards, A. M. and Bees, M. A.: Generic dynamics of a simple plankton population model with a non-integer exponent of closure, Chaos Solitons Fractals, 12, 289–300, 2001.
Eiane, K., Aksnes, D. L., Ohman, M. D., Wood, S., and Martinussen, M. B.: Stage-specific mortality of Calanus spp. under different predation regimes, Limnol. Oceanogr., 47, 636–645, 2002.
Fasham, M. J. R., Ducklow, H. W., and McKelvie, S. M.: A nitrogen-based model of plankton dynamics in the oceanic mixed layer, J. Mar. Res., 48, 591–639, 1990.
Forest, A., Stemmann, L., Picheral, M., Burdorf, L., Robert, D., Fortier, L., and Babin, M.: Size distribution of particles and zooplankton across the shelf-basin system in southeast Beaufort Sea: combined results from an Underwater Vision Profiler and vertical net tows, Biogeosciences, 9, 1301–1320, doi:10.5194/bg-9-1301-2012, 2012.
Frey, K. E, McClelland, J. W., Holmes, R. M., and Smith, L. C.: Impacts of climate warming and permafrost thaw on the riverine transport of nitrogen and phosphorus to the Kara Sea, J. Geophys. Res.-Biogeo., 112, G04S58, doi:10.1029/2006JG000369, 2007.

BGD
11, 16953–16992, 2014

Garneau, M. E., Roy, S., Lovejoy, C., Gratton, Y., and Vincent, W. F.: Seasonal dynamics of bacterial biomass and production in a coastal arctic ecosystem: Franklin Bay, western Canadian Arctic, J. Geophys. Res., 113, C07S91, doi:10.1029/2007JC004281, 2008.

Geider, R. J., MacIntyre, H. L., and Kana, T. M.: Dynamic model of phytoplankton growth and acclimation: responses of the balanced growth rate and the chlorophyll a: carbon ratio to light, nutrient-limitation and temperature, Mar. Ecol.-Prog. Ser., 148, 187–200, 1997.

Guerrero, M. A. and Jones, R. D.: Photoinhibition of marine nitrifying bacteria, II. Dark recovery after monochromatic or polychromatic irradiation, Mar. Ecol.-Prog. Ser., 141, 193–198, 1996.

Grossart, H.-P. and Ploug, H.: Microbial degradation of organic carbon and nitrogen on diatom aggregates, Limnol. Oceanogr., 46, 267–277, 2001.

Hibler III, W. D.: A dynamic thermodynamic sea ice model, J. Phys. Oceanogr., 9, 815–846, 1979.

Hibler III, W. D. and Bryan, K.: A diagnostic ice–ocean model, J. Phys. Oceanogr., 17, 987–1015, 1987.

Hill, V. J., Matrai, P., Olson, E., Suttle, S., Steele, M., Codispoti, L., and Zimmerman, R.: Synthesis of integrated primary production in the Arctic Ocean: II. In situ and remotely sensed estimates, Prog. Oceanogr., 110, 107–125, doi:10.1016/j.pocean.2012.11.005, 2013.

Holmes, R. M., McClelland, J. W., Peterson, B. J., Tank, S. E., Bulygina, E., Eglinton, T. I., Gordeev, V. V., Gurtovaya, T. Y., Raymond, P. A., Repeta, D. J., Staples, R., Stiegl, R. G., Zhulidov, A. V., and Zimov, S. A.: Seasonal and annual fluxes of nutrients and organic matter from large rivers to the Arctic Ocean and surrounding seas, Estuar. Coast., 35, 369–382, doi:10.1007/s12237-011-9386-6, 2011.

Jakobsson, M., Macnab, R., Mayer, L., Anderson, R., Edwards, M., Hatzky, J., Schenke, H. W., and Johnson, P.: An improved bathymetric portrayal of the Arctic Ocean: implications for ocean modeling and geological, geophysical and oceanographic analyses, Geophys. Res. Lett., 35, L07602, doi:10.1029/2008GL033520, 2008.

Kahru, M., Brotas, V., Manzano-Sarabia, M., and Mitchell, B. G.: Are phytoplankton blooms occurring earlier in the Arctic?, Glob. Change Biol., 17, 1733–1739, doi:10.1111/j.1365-2486.2010.02312.x, 2011.

Kichman, D. L., Kiel, R. G., and Wheeler, P. A.: The effect of amino acids on ammonium utilization and regeneration by heterotrophic bacteria in the subarctic Pacific, Deep-Sea Res., 36, 1763–1776, 1989.

BGD
11, 16953–16992, 2014

Kirchman, D. L.: Limitation of bacterial growth by dissolved organic matter in the subarctic Pacific, Mar. Ecol.-Prog. Ser., 62, 47–54, 1990.

Kirchman, D. L., Malmstrom, R. R., and Cottrell, M. T.: Control of bacterial growth by temperature and organic matter in the Western Arctic, Deep-Sea Res. Pt. II, 52, 3386–3395, doi:10.1016/j.dsr2.2005.09.005, 2005.

Kirchman, D. L., Hill, V., Cottrell, M. T., Gradinger, R., Malmstrom, R. R., and Parker, A.: Standing stocks, production, and respiration of phytoplankton and heterotrophic bacteria in the western Arctic Ocean, Deep-Sea Res. Pt. II, 56, 1237–1248, doi:10.1016/j.dsr2.2008.10.018, 2009.

Köhler, H., Meon, B., Gordeev, V. V., Spitzy, A., and Amon, R. M. W.: Dissolved organic matter (DOM) in the estuaries of Ob and Yenisei and the adjacent Kara Sea, Russia, in: Siberian River Run-off in the Kara Sea: Characterisation, Quantification, Variability, and Environmental Significance, Proceedings in Marine Sciences, 6, edited by: Stein, R., Fahl, K., Fütterer, D. K., Galimov, E. M., and Stepanets, O. V., Elsevier, Amsterdam, 281–308, 2003.

Kristiansen, S., Fabrot, T., and Wheeler, P. A.: Nitrogen cycling in the Barents Sea – Seasonal dynamics of new and regenerated production in the Marginal Ice Zone, Limnol. Oceanogr., 39, 1630–1642, 1994.

Lammers, R. B., Shiklomanov, A. I., Vörösmarty, C. J., Fekete, B. M., and Peterson, B. J.: Assessment of contemporary Arctic river runoff based on observational discharge records, J. Geophys. Res., 106, 3321–3334, 2001.

Lancelot, C., Becquevort, S., Menon, P., Mathot, S., and Dandois, J.-M.: Ecological modelling of the planktonic microbial food-web, in: Belgian Research Program on the Antarctic, Scientific Results of Phase III (1992–1996): Marine Biogeochemistry and Ecodynamics, vol. 1, edited by: Caschetto, S., Fed. Off. for Sci., Tech., and Cult. Affairs, Brussels, 1–78, 1997.

Le Fouest, V., Zakardjian, B., Saucier, F. J., and Starr, M.: Seasonal vs. synoptic variability in planktonic production in a high-latitude marginal sea: the Gulf of St. Lawrence (Canada), J. Geophys. Res., 110, C099012, doi:10.1029/2004JC002423, 2005.

Le Fouest, V., Zakardjian, B., Saucier, F. J., and Cizmeli, S. A.: Application of SeaWIFS- and AVHRR-derived data for mesoscale and regional validation of a 3-D high-resolution physical-biological model of the Gulf of St. Lawrence (Canada), 2006, J. Marine Syst., 60, 30–50, 2006.

BGD
11, 16953–16992, 2014

Le Fouest, V., Postlethwaite, C., Morales Maqueda, M. A., Bélanger, S., and Babin, M.: On the role of tides and strong wind events in promoting summer primary production in the Barents Sea, Cont. Shelf Sci., 31, 1869–1879, doi:10.1016/j.csr.2011.08.013, 2011.

Le Fouest, V., Babin, M., and Tremblay, J.-É.: The fate of riverine nutrients on Arctic shelves, Biogeosciences, 10, 3661–3677, doi:10.5194/bg-10-3661-2013, 2013a.

Le Fouest, V., Zakardjian, B., Xie, H., Raimbault, P., Joux, F., and Babin, M.: Modeling plankton ecosystem functioning and nitrogen fluxes in the oligotrophic waters of the Beaufort Sea, Arctic Ocean: a focus on light-driven processes, Biogeosciences, 10, 4785–4800, doi:10.5194/bg-10-4785-2013, 2013b.

Lehrter, J. C., Pennock, J. R., and McManus, G. B.: Microzooplankton grazing and nitrogen excretion across a surface estuarine-coastal interface, Estuaries, 22, 113–125, 1999.

Letscher, R. T., Moore, J. K., Teng, Y.-C., and Primeau, F.: Variable C: N: P stoichiometry of dissolved organic matter cycling in the Community Earth System Model, Biogeosciences Discuss., 11, 9071–9101, doi:10.5194/bgd-11-9071-2014, 2014.

Li, W. K. W., McLaughlin, F. A., Lovejoy, C., and Carmack, E. C.: Smallest algae thrive as the Arctic Ocean freshens, Science, 326, 539, doi:10.1126/science.1179798, 2009.

Nedwell, D. B. and Rutter, M.: Influence of temperature on growth rate and competition between two psychrotolerant antarctic bacteria: low temperature diminishes affinity for substrate uptake, Appl. Environ. Microb., 60, 1984–1992, 1994.

Manizza, M., Follows, M. J., Dutkiewicz, S., McClelland, J. W., Menemenlis, D., Hill, C. N., Townsend-Small, A., and Peterson, B. J.: Modeling transport and fate of riverine dissolved organic carbon in the Arctic Ocean, Global Biogeochem. Cy., 23, GB4006, doi:10.1029/2008GB003396, 2009.

Manizza, M., Follows, M. J., Dutkiewicz, S., Menemenlis, D., Hill, C. N., and Key, R. M.: Changes in the Arctic Ocean CO_2 sink (1996–2007): a regional model analysis, Global Biogeochem. Cy., 27, 1108–1118, doi:10.1002/2012GB004491, 2013.

Mann, P. J., Davydova, A., Zimov, N., Spencer, R. G. M., Davydov, S., Bulygina, E., Zimov, S., and Holmes, R. M.: DOM composition and lability during the Arctic spring freshet on the River Kolyma, Northeast Siberia, J. Geophys. Res., 117, G01028, doi:10.1029/2011JG001798, 2012.

Marshall, J., Hill, C., Perelman, L., and Adcroft, A.: Hydrostatic, quasi-hydrostatic and nonhydrostatic ocean modeling, J. Geophys. Res., 102, 5733–5752, 1997.

BGD
11, 16953–16992, 2014

McClelland, J. W., Holmes, R. M., Peterson, B. J., Amon, R., Brabets, T., Cooper, L., Gibson, J., Gordeev, V. V. Guay, C., Milburn, D., Staples, R., Raymond, P. A., Shiklomanov, I., Striegl, R., Zhulidov, A., Gurtovaya, T., and Zimov, S.: Development of a pan-Arctic database for river chemistry, Eos Trans. AGU, 89, 217, doi:10.1029/2008EO240001, 2008.

MacIntyre, H. L., Kana, T. M., Anning, T., and Geider, R. J.: Photoacclimation of photosynthesis irradiance response curves and photosynthetic pigments in microalgae and cyanobacteria, J. Phycol., 38, 17–38, 2002.

Menemenlis, D., Hill, C., Adcroft, C. A., Campin, J.-M., Cheng, B., Ciotti, B., Fukumori, I., Heimbach, P., Henze, C., Kohl, A., Lee, T., Stammer, D., Taft, J., and Zhang, J.: NASA supercomputer improves prospects for ocean climatic research, Eos Trans. AGU, 86, 89–96, 2005.

Meon, B. and Amon, R. M. W.: Heterotrophic bacterial activity and fluxes of dissolved free amino acids and glucose in the Arctic rivers Ob, Yenisei and the adjacent Kara Sea, Aquat. Microb. Ecol., 37, 121–135, 2004.

Morel, A.: Optical modeling of the upper ocean in relation to its biogenous matter content (case I waters), J. Geophys. Res., 93, 10749–10768, 1988.

National Oceanographic Data Centre World Ocean Atlas 2005: Documentation accompanying WOA05 DVD (ASCII text and portable document format), Prepared by the Ocean Climate Laboratory, National Oceanographic Data Center, Silver Springs, MD 20910, 12 pp., 2006.

Ohman, M. D., Eiane, K., Durbin, E. G., Runge, J. A., and Hirche, H.-J.: A comparative study of Calanus finmarchicus mortality patterns at five localities in the North Atlantic, ICES J. Mar. Sci., 61, 687–697, 2004.

Olson, R. J.: Differential photoinhibition of marine nitrifying bacteria: a possible mechanism for the formation of the primary nitrite maximum, J. Mar. Res., 39, 227–238, 1981a.

Olson, R. J.: 15N tracers studies of the primary nitrite maximum, J. Mar. Res., 39, 203–226, 1981b.

O'Neill, R. V., DeAngelis, D. L., Pastor, J. J., Jackson, B. J., and Post, W. M.: Multiple nutrient limitations in ecological models, Ecol. Model., 46, 147–163, 1989.

Onogi, K., Tsutsui, J., Koide, H., Sakamoto, M., Kobayashi, S., Hatsushika, H., Matsumoto, T., Yamazaki, N., Kamahori, H., Takahashi, K., Kadokura, S., Wada, K., Kato, K., Oyama, R., Ose, T., Mannoji, N., and Taira, R.: The JRA-25 reanalysis, J. Meteorol. Soc. Jpn., 85, 369–432, 2007.

Opsahl, S., Benner, R., and Amon, R. M. W.: Major flux of terrigenous dissolved organic matter through the Arctic Ocean, Limnol. Oceanogr., 44, 2017–2023, 1999.

BGD
11, 16953–16992, 2014

Ortega-Retuerta, E., Jeffrey, W. H., Babin, M., Bélanger, S., Benner, R., Marie, D., Matsuoka, A., Raimbault, P., and Joux, F.: Carbon fluxes in the Canadian Arctic: patterns and drivers of bacterial abundance, production and respiration on the Beaufort Sea margin, Biogeosciences, 9, 3679–3692, doi:10.5194/bg-9-3679-2012, 2012.

Piontek, J., Sperling, M., Nothig, E.-M., and Engel, A.: Regulation of bacterioplankton activity in Fram Strait (Arctic Ocean) during early summer: the role of organic matter supply and temperature, J. Marine Syst., 132, 83–94, 2014.

Rachold, V., Eiken, H., Gordeev, V. V., Grigoriev, M. N., Hubberten, H.-W., Lisitzin, A. P., Shevchenko, V. P., and Schirmeister, L.: Modern terrigenous organic carbon input to the Arctic Ocean, in: The Organic Carbon Cycle in the Arctic Ocean, edited by: Stein, R. S. and Macdonald, R. W., Springer, New York, 33–55, 2004.

Raymond, P. A., McClelland, J. W., Holmes, R. M., Zhulidov, A. V., Mull, K., Peterson, B. J., Striegl, R. G., Aiken, G. R., and Gurtovaya, T. Y.: Flux and age of dissolved organic carbon exported to the Arctic Ocean: a carbon isotopic study of the five largest arctic rivers, Global Biogeochem. Cy., 21, GB4011, doi:10.1029/2007GB002934, 2007.

Redfield, A. C., Ketchum, B. H., and Richards, F. A.: The influence of organisms on the composition of sea water, in: The Sea: Ideas and Observations on Progress in the Study of the Seas, edited by: Hill, M. N., Wiley-Intersci., Hoboken, NY, 26–27, 1973.

Rich, J., Gosselin, M., Sherr, E., Sherr, B., and Kirchman, D. L.: High bacterial production, uptake and concentrations of dissolved organic matter in the Central Arctic Ocean, Deep-Sea Res. Pt. II, 44, 1645–1663, doi:10.1016/S0967-0645(97)00058-1, 1997.

Riegman, R., Kuipers, B. R., Nooedeloos, A. A. M., and Witte, H. J.: Size-differential control of phytoplankton and the structure of plankton communities, Neth. J. Sea Res., 31, 255–265, 1993.

Sakshaug, E.: Primary and secondary production in the Arctic Seas, in: The Organic Carbon Cycle in the Arctic Ocean, edited by: Stein, R. and Macdonald, R. W., Springer, Berlin, Heidelberg, 57–81, doi:10.1007/978-3-642-18912-8_3, 2004.

Sahzin, A. F., Romanova, N. D., and Mosharov, S. A.: Bacterial and primary production in the pelagic zone of the Kara Sea, Oceanology, 50, 759–765, 2010.

Serreze, M., Barret, A. P., Slater, A. G., Woodgate, R. A., Aagard, K., Lammers, R. B., Steele, M., Mortitz, R., Meredith, M., and Lee, C. M.: The large-scale fresh water cycle of the Arctic, J. Geophys. Res., 111, C11010, doi:10.1029/2005JC003424, 2006.

BGD
11, 16953–16992, 2014

Sherr, E. B., Sherr, B. F., Wheeler, P. A., and Thompson, K.: Temporal and spatial variation in stocks of autotrophic and heterotrophic microbes in the upper water column of the central Arctic Ocean, Deep-Sea Res. Pt. I, 50, 557–571, doi:10.1016/S0967-0637(03)00031-1, 2003.

Shiklomanov, A. and Lammers, R. B.: River discharge (in: Arctic, Report Card 2011), available at: http://www.arctic.noaa.gov/report11/river_discharge.html (last access: 27 October 2014), 2011.

Shiklomanov, I., Shiklomanov, A., Lammers, R., Peterson, B., and Vorosmarty, C.: The dynamics of river water inflow to the Arctic Ocean, in: The Freshwater Budget of the Arctic Ocean, edited by: Lewis, E., Kluwer Acad., Dordrecht, the Netherlands, 281–296, 2000.

Sibert, V., Zakardjian, B., Gosselin, M., Starr, M., Senneville, S., LeClainche, Y.: 3-D bio-physical model of the sympagic and planktonic productions in the Hudson Bay System, J. Marine Syst., 88, 401–422, doi:10.1016/j.jmarsys.2011.03.014, 2011.

Simpson, K. G., Tremblay, J.-É, Brugel, S., and Price, N. M.: Nutrient dynamics in the western Canadian Arctic, II. Estimates of new and regenerated production over the Mackenzie Shelf and Cape Bathurst Polynya, Mar. Ecol.-Prog. Ser., 484, 47–62, doi:10.3354/meps10298, 2013.

Steele, J. H. and Henderson, E. W.: The role of predation in plankton models, J. Plankton Res., 14, 157–172, 1992.

Steele, M., Morley, R., and Ermold, W.: PHC: a global ocean hydrography with a high quality Arctic Ocean, J. Climate, 14, 2079–2087, doi:10.1175/1520-0442(2001)014<2079:PAGOHW>2.0.CO;2, 2001.

Steele, M., Ermold, W., and Zhang, J.: Arctic Ocean surface warming trends over the past 100,years, Geophys. Res. Lett., 35, L02614, doi:10.1029/2007GL031651, 2008.

Steward, G. F., Smith, D. C., and Azam, F.: Abundance and production of bacteria and viruses in the Bering and Chukchi Seas, Mar. Ecol.-Prog. Ser., 131, 287–300, 1996.

Sturluson, M., Nielsen, T. G., and Wassmann, P.: Bacteria abundance, biomass and production during spring blooms in the northern Barents Sea, Deep-Sea Res. Pt. II, 55, 2186–2198, 2008.

Taniguchi, A.: Differences in structure of lower trophic levels of pelagic ecosystems in the eastern and western subarctic Pacific, Prog. Oceanogr., 43, 289–315, 1999.

BGD
11, 16953–16992, 2014

Tank, S. E., Manizza, M., Holmes, R. M., McClelland, J. W., and Peterson, B. J.: The processing and impact of dissolved riverine nitrogen in the Arctic Ocean, Estuar. Coast., 35, 401–415, doi:10.1007/s12237-011-9417-3, 2012.

Thingstad, T, F., Bellerby, R. G. J., Bratbak, G., Børsheim, K. Y., Egge, J. K., Heldal, M., Larsen, A., Neill, C., Nejstgaard, J., Norland, S., Sandaa, R.-A., Skjoldal, E., Tanaka T, T., Thyrhaug, R., and Töpper, B.: Counterintuitive carbon-to-nutrient coupling in an Arctic pelagic ecosystem, Nature, 455, 387–390, 2008.

Timmermans, M.-L., Ashik, I., Cao, Y., Frolov, I., Ha, H. K., Ingvaldsen, R., Kikuchi, T., Kim, T. W., Krishfield, R., Loeng, H., Nishino, S., Pickart, R., Polyakov, I., Rabe, B., Semiletov, I., Schauer, U., Schlosser, P., Shakhova, N., Smethie, W. M., Sokolov, V., Steele, M., Su, J., Toole, J., Williams, W., Woodgate, R., Zhao, J., Zhong, W., and Zimmermann, S: Arctic Ocean Sea Surface Temperature (in: Arctic Report Card), available at: http://www.arctic.noaa.gov/reportcard/ocean_temperature_salinity.html (last access: 3 December 2014), 2014.

Tremblay, J.-É., Legendre, L., Klein, B., and Therriault, J.-C.: Size differential uptake of nitrogen and carbon in a marginal sea (Gulf of St. Lawrence, Canada): significance of diel periodicity and urea uptake, Deep-Sea Res. Pt. II, 47, 489–518, 2000.

Vancoppenolle, M., Bopp, L., Madec, G., Dunne, J., Ilyina, T., Halloran, P. R., and Steiner, N.: Future Arctic Ocean primary productivity from CMIP5 simulations: Uncertain outcome, but consistent mechanisms, Global Biogeochem. Cy., 27, 605–619, doi:10.1002/gbc.20055, 2013.

Vallières C., Retamal, L., Osburn, C., and Vincent, W. F.: Bacterial production and microbial food web structure in a large Arctic river and the coastal Arctic Ocean, J. Marine Syst., 74, 756–773, doi:10.1016/j.jmarsys.2007.12.002, 2008.

Wickland, K. P., Aiken, G. R., Butler, K., Dornblaser, M. M., Spencer, R. G. M., and Striegl, R. G.: Biodegradability of dissolved organic carbon in the Yukon River and its tributaries: seasonality and importance of inorganic nitrogen, Global Biogeochem. Cy., 26, GB0E03, doi:10.1029/2012GB004342, 2012.

Xie, H., Bélanger, S., Song, G., Benner, R., Taalba, A., Blais, M., Tremblay, J.-É., and Babin, M.: Photoproduction of ammonium in the southeastern Beaufort Sea and its biogeochemical implications, Biogeosciences, 9, 3047–3061, doi:10.5194/bg-9-3047-2012, 2012.

Zhang, J. and Hibler III, W. D.: On an efficient numerical method for modeling sea ice dynamics, J. Geophys. Res., 102, 8691–8702, 1997.

BGD
11, 16953–16992, 2014

Zhang, J. and Rothrock, D.: Modeling global sea ice with a thickness and enthalpy distribution model in generalized curvilinear coordinates, Mon. Weather Rev., 131, 845–861, doi:10.1175/1520-0493(2003)131<0845:MGSIWA>2.0.CO;2, 2003.

BGD
11, 16953–16992, 2014

Table 1. Differential equations for the 10-component biogeochemical model: nitrate (NO_3), ammonium (NH_4), large and small phytoplankton (LP and SP, respectively), large and small zooplankton (LZ and SZ, respectively), bacterioplankton (BACT), detrital particulate and dissolved organic nitrogen (dPON and dDON, respectively), and usable riverine dissolved organic nitrogen (RDON).

$$\frac{\partial NO_3}{\partial t} = -\nabla\cdot(\mathbf{u}NO_3 - \mathbf{K}\cdot\nabla NO_3) + \text{nitrif} - \text{lim}^{LP}_{NO_3}\mu_{LP}LP - \text{lim}^{SP}_{NO_3}\mu_{SP}SP$$

$$\frac{\partial NH_4}{\partial t} = -\nabla\cdot(\mathbf{u}NH_4 - \mathbf{K}\cdot\nabla NH_4) - \text{lim}^{LP}_{NH_4}\mu_{LP}LP - \text{lim}^{SP}_{NH_4}\mu_{SP}SP - \text{nitrif} - \text{Ubact}_{NH_4}\text{BACT}(1-\text{ge}_{BACT}) + \text{eg}_{SZ}(1-\text{ge}_{SZ})G_{SZ}SZ + \text{ex}_{LZ}LZ$$

$$\frac{\partial LP}{\partial t} = -\nabla\cdot(\mathbf{u}LP - \mathbf{K}\cdot\nabla LP) + \mu_{LP}LP - G_{LZ}\text{pf}_{LP}LZ - m_{LP}LP + \frac{\partial}{\partial z}\left(\text{sed}_{lp}LP\right)$$

$$\frac{\partial SP}{\partial t} = -\nabla\cdot(\mathbf{u}SP - \mathbf{K}\cdot\nabla SP) + \mu_{SP}SP - G_{SZ}\text{pf}_{SP}SZ - m_{SP}SP$$

$$\frac{\partial LZ}{\partial t} = -\nabla\cdot(\mathbf{u}LZ - \mathbf{K}\cdot\nabla LZ) + \text{assim}_{LZ}G_{LZ}LZ - m_{LZ}LZ^2 - \text{ex}_{LZ}LZ$$

$$\frac{\partial SZ}{\partial t} = -\nabla\cdot(\mathbf{u}SZ - \mathbf{K}\cdot\nabla SZ) + \text{assim}_{SZ}G_{SZ}SZ - m_{SZ}SZ^2 - G_{LZ}(1-\text{pf}_{LP})LZ$$

$$\frac{\partial BACT}{\partial t} = -\nabla\cdot(\mathbf{u}BACT - \mathbf{K}\cdot\nabla BACT) + \text{Ubact}_{NH_4}\text{BACTge} + \text{Ubact}_{dDONl}\text{BACTge}_{BACT} - m_{BACT}BACT - G_{SZ}(1-\text{pf}_{SP})SZ$$

$$\frac{\partial dPON}{\partial t} = -\nabla\cdot(\mathbf{u}dPON - \mathbf{K}\cdot\nabla dPON) + (1-\text{assim}_{LZ})G_{LZ}LZ + m_{LZ}LZ^2 + m_{LP}LP + \frac{\partial}{\partial z}\left(\text{sed}_{dpon}dPON\right) - f_g dPON$$

$$\frac{\partial dDON}{\partial t} = -\nabla\cdot(\mathbf{u}dDON - \mathbf{K}\cdot\nabla dDON) + f_g dPON + m_{SZ}SZ^2 + m_{SP}SP + m_{BACT}BACT + (1-\text{eg}_{SZ})(1-\text{ge}_{SZ})G_{SZ}SZ - \text{Ubact}_{DONl}\text{BACTpf}_{DONl}(1-\text{ge}_{BACT})$$

$$\frac{\partial RDON}{\partial t} = -\nabla\cdot(\mathbf{u}RDON - \mathbf{K}\cdot\nabla RDON) - \text{Ubact}_{DONl}\text{BACT}(1-\text{pf}_{DONl})\left(1/\text{ratio}_{CN}\right)(1-\text{ge}_{BACT})$$

BGD
11, 16953–16992, 2014

Table 2. Biogeochemical model parameters.

Symbol	Description	Value	Units
Nutrients			
$\text{nitrif}_{\max}$	Maximum NH_4 nitrification rate	0.05	d^{-1}
K_{nitrif}^{N}	Half-saturation constant for NH_4 nitrification	0.07	mmol N m^{-3}
Phytoplankton			
k_w	Light attenuation coefficient due to water	0.04	m^{-1}
k_{nonchl}	Light attenuation coefficient due to nonchlorophyllous matter	0.05	m^{-1}
$K_{NO_3}^{LP}$	Half-saturation constant for NO_3 use by LP	1	mmol N m^{-3}
$K_{NO_3}^{SP}$	Half-saturation constant for NO_3 use by SP	1	mmol N m^{-3}
$K_{NH_4}^{LP}$	Half-saturation constant for NH_4 use by LP	0.5	mmol N m^{-3}
$K_{NH_4}^{SP}$	Half-saturation constant for NH_4 use by SP	0.1	mmol N m^{-3}
K_E^{LP}	Photoacclimation parameter	8	$\text{Ein m}^{-2}\,\text{d}^{-1}$
K_E^{SP}	Photoacclimation parameter	4	$\text{Ein m}^{-2}\,\text{d}^{-1}$
$\left(\frac{\text{Chl}}{\text{C}}\right)_{\max}^{LP}$	Maximum Chl to C ratio for LP	0.0125	g g^{-1}
$\left(\frac{\text{Chl}}{\text{C}}\right)_{\max}^{SP}$	Maximum Chl to C ratio for SP	0.07	g g^{-1}
$\mu_{\max}^{LP}$	Maximum growth rate for LP	1.4	d^{-1}
$\mu_{\max}^{SP}$	Maximum growth rate for SP	1.4	d^{-1}
α_{SP}	Initial slope of the photosynthesis-irradiance curve	5.5	$\text{mg C (mg Chl)}^{-1}\,(\text{Ein m}^{-2}\,\text{d}^{-1})^{-1}$
α_{LP}	Initial slope of the photosynthesis-irradiance curve	7.5	$\text{mg C (mg Chl)}^{-1}\,(\text{Ein m}^{-2}\,\text{d}^{-1})^{-1}$
sed_lp	LP sinking rate	2	m^{-1}
m_{LP}	LP basal mortality	0.05	d^{-1}
m_{SP}	SP basal mortality	0.05	d^{-1}
Zooplankton			
$G_{LZ}^{\max}$	Maximum grazing rate for LZ	0.3	d^{-1}
λ	Ivlev constant for LZ	0.5	$(\text{mmol N m}^{-3})^{-1}$
$G_{SZ}^{\max}$	Maximum grazing rate for SZ	1	d^{-1}
K_G	Half-saturation constant for SZ grazing	0.8	mmol N m^{-3}
assim_{LZ}	LZ assimilation efficiency	70	%
ge_{SZ}	SZ growth efficiency	30	%
eg_{SZ}	dDON egestion by SZ	40	%
ex_{LZ}	NH_4 excretion by LZ	0.05	d^{-1}
m_{SZ}	SZ mortality	0.05	$(\text{mmol N m}^{-3})^{-1}$
m_{LZ}	LZ mortality	0.2	$(\text{mmol N m}^{-3})^{-1}$
Bacterioplankton			
$\text{Ubact}_{\max}$	Maximum growth rate	1	d^{-1}
$K_{NH_4}^{BACT}$	Half-saturation constant for NH_4 uptake	0.1	mmol N m^{-3}
K_{DONI}^{BACT}	Half-saturation constant for DONI uptake	0.1	mmol N m^{-3}
ge_{BACT}	Growth efficiency	20	%
m_{BACT}	Basal mortality	0.05	d^{-1}
Detritus			
sed_dpon	dPON sinking rate	100	$\text{m d}^{-1}\,(\text{mmol N m}^{-3})^{-1}$
f_g	dPON fragmentation	0.05	d^{-1}
RDON			
ratio_{CN}	Carbon to Nitrogen ratio	40 : 1	mol mol^{-1}

BGD
11, 16953–16992, 2014

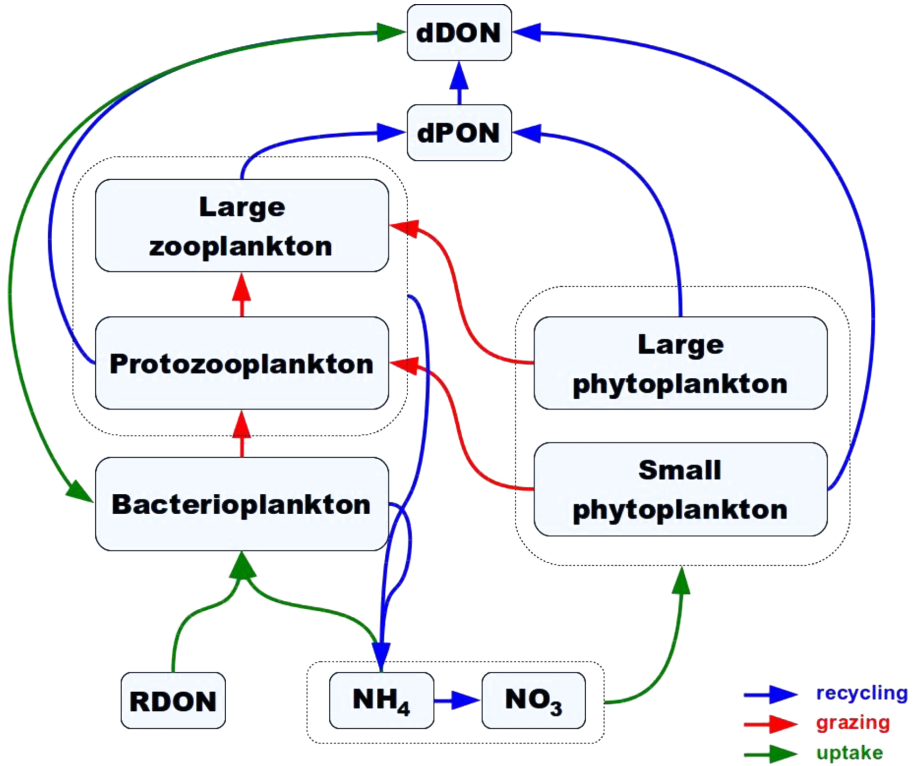

Figure 1. Conceptual diagram of the biogeochemical model. The 10 state variables are nitrate (NO_3), ammonium (NH_4), large (> 5µm) and small (< 5µm) phytoplankton, large zooplankton, protozooplankton, bacterioplankton, detrital particulate and dissolved organic nitrogen (dPON and dDON, respectively), and usable riverine dissolved organic nitrogen (RDON). Green, red and blue arrows represent nutrients uptake, grazing and nitrogen recycling, respectively.

BGD
11, 16953–16992, 2014

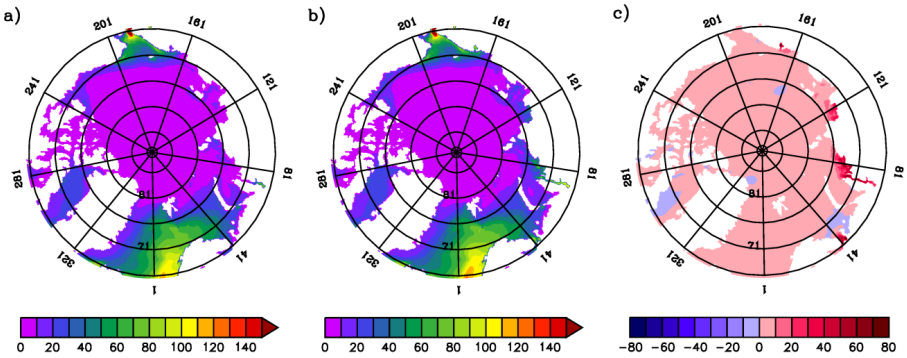

Figure 2. Mean annual ocean primary production (gC m^{-2}) over 1998–2011 **(a)** without RDON removal by bacterioplankton (CTRL run), **(b)** with RDON removal by bacterioplankton (RIV run), and **(c)** absolute difference (gC m^{-2}; RIV run – CTRL run).

BGD
11, 16953–16992, 2014

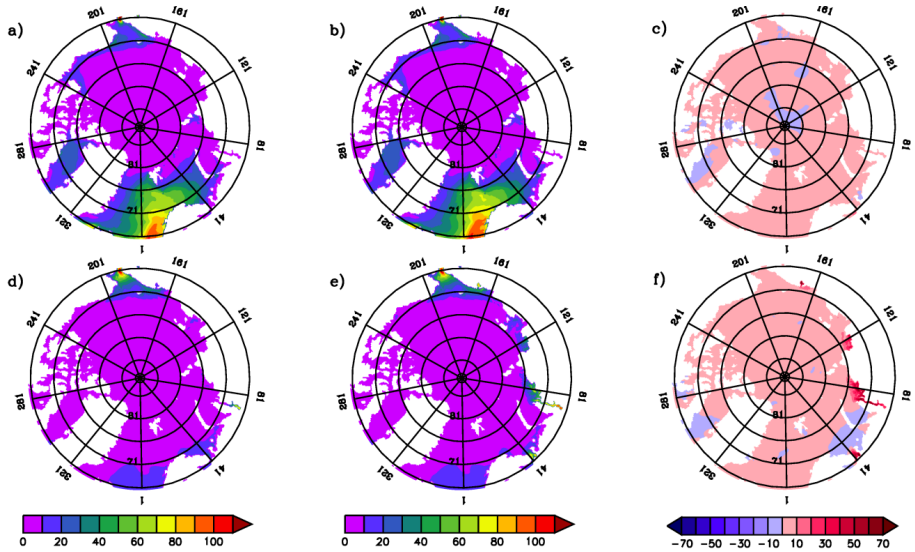

Figure 3. Mean annual new primary production ($gC\,m^{-2}$; upper panels) and NH_4-supported primary production ($gC\,m^{-2}$; lower panels) over 1998–2011 simulated in CTRL run (**a** and **d**) and in RIV run (**b** and **e**). Right panels (**c** and **f**) provide the absolute difference ($gC\,m^{-2}$; RIV run – CTRL run).

BGD
11, 16953–16992, 2014

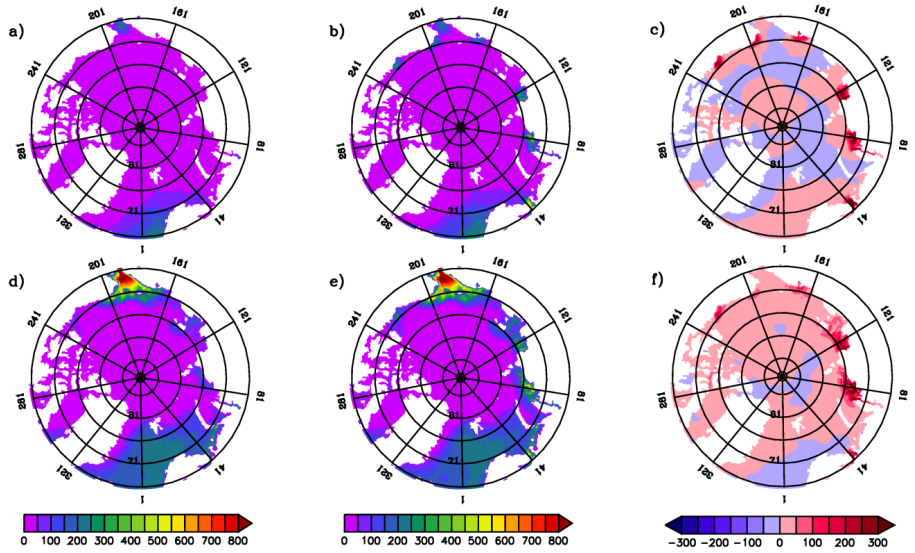

Figure 4. Seasonal climatology of the 0–50 m integrated bacterial biomass (mmol N m^{-2}) for spring (upper panels) and summer (lower panels) over the 1998–2011 period simulated in CTRL run (**a** and **d**) and in RIV run (**b** and **e**). Right panels (**c** and **f**) provide the absolute difference (g C m^{-2}; RIV run – CTRL run).

BGD
11, 16953–16992, 2014

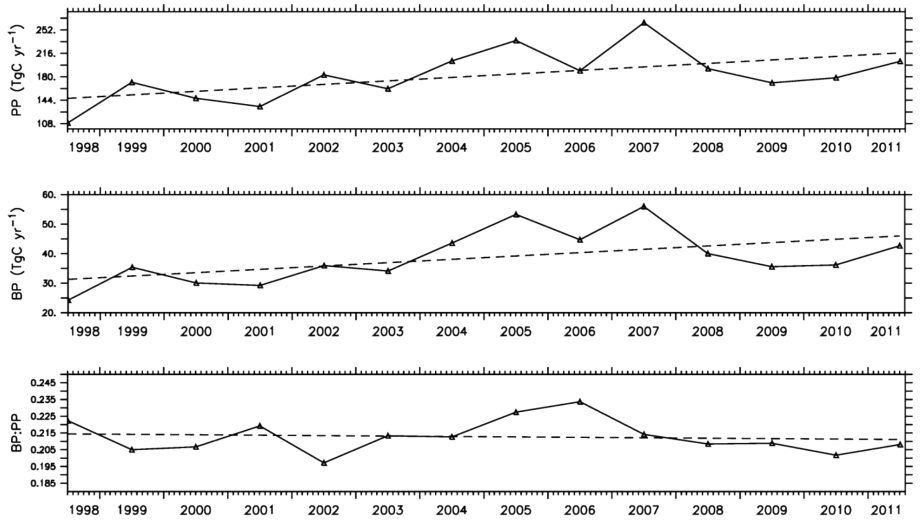

Figure 5. Time course of primary production (PP, Tg C yr^{-1}) (top panel), bacterioplankton production (BP, Tg C yr^{-1}) (middle panel), and of the BP : PP ratio in the ice-free shelves (see text for details) of the Arctic Ocean domain (> 66.5° N) simulated in RIV run. The dashed straight lines represent the linear trend computed over the 1998–2011 period.

BGD
11, 16953–16992, 2014